CRYSTAL GROWTH & DESIGN

pubs.acs.org/crystal

Article

Solvent-Dependent Self-Assembly of Hydrogen-Bonded Organic Porphyrinic Frameworks

Li Ma, Hadi Arman, Yi Xie,* Wei Zhou, and Banglin Chen*

Cite This: *Cryst. Growth Des.* 2022, 22, 3808−3814

Read Online

ACCESS | Metrics & More | Article Recommendations | Supporting Information

ABSTRACT: Three hydrogen-bonded organic frameworks (HOFs) (**HOF-26**, **HOF-27**, **HOF-28**) have been crystallized from a benzonitrile-based porphyrinic organic linker 4,4′,4″,4‴-(porphyrin-5,10,15,20-tetrayl)tetrabenzonitrile (PTTBN), in ethylbenzene, nitrobenzene, and tetrahydrofuran, respectively, and structurally characterized. Close inspection of the crystal structure of the HOFs reveals that PTTBN units form a two-dimensional hydrogen-bonded sql network but with varied hydrogen bonding connectivities, packing patterns, and host−guest interactions. The pore system in these HOFs can be systematically modulated by the guest molecules and tuned from discrete cavities to one-dimensional channels with distinct dimensions. Energy decomposition analysis was carried out to investigate the intralayer and interlayer interaction energy to understand the solvent-dependent self-assembly.

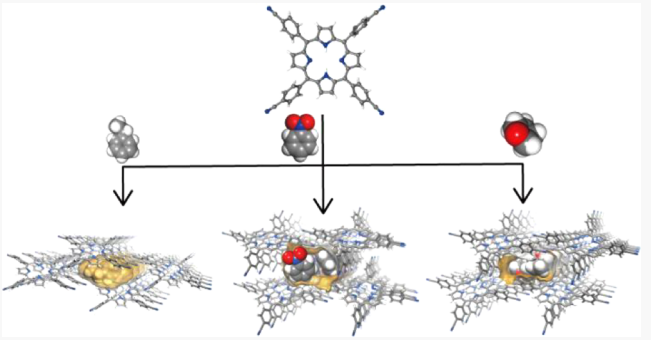

INTRODUCTION

Hydrogen-bonding-directed self-assembly is a crucial process in biological systems to form ordered molecular structures.[1] Hydrogen-bonded organic frameworks (HOFs), an emerging class of crystalline porous materials, are held together by organic units through hydrogen bonding interactions.[2−5] Compared with covalent bonds and coordination bonds, as shown in covalent organic frameworks (COFs)[6] and metal−organic frameworks (MOFs),[7,8] the bonding energy of hydrogen bonds is intrinsically low, which sets significant challenges in the design and synthesis of robust HOFs. The applications of HOFs had been limited for decades due to their fragility until recent discoveries in many promising applications using robust HOFs such as gas separation,[9−14] chiral separation,[15] heterogeneous catalysis,[16−18] sensing,[19,20] and enzyme encapsulation.[21] The rapid growth in HOF chemistry has attracted much attention, thanks to its large surface area, tunable pore environment, and easy regeneration by recrystallization.[22−25] In addition, the metal-free characteristic of HOFs shows excellent potential in biomedical applications considering its low toxicity and excellent biocompatibility.

The quest for rational design and precise prediction of HOF structures is obstructed by the liability and low directionality of weak hydrogen bonds and insufficient understanding of the molecular self-assembly mechanism, namely, the energy−structure relationship.[26] Thereby, organic units with the potential for strong hydrogen bonds with high directionality have been utilized as the backbone for the construction of HOF architectures, as exemplified by some representative building blocks such as 2,4-diaminotriazine (DAT),[27−30] carboxylic acid,[31−34] pyrazole,[35,36] imidazole,[37] guanidinium-sulfonate,[14,38] pyridine,[9,39] and even nitrobenzo[40] and aldehyde group.[41] On the other hand, starting from the same linker, the self-assembly and the functionalities of the HOF structure can also be significantly affected by solvent molecules due to the resultant different hydrogen-bonded network connectivities or interpenetration patterns.[33,42,43] Recently, we demonstrated unprecedented ethylene/ethane separation performance and exclusive *p*-xylene molecular recognition from C8 mixtures in benzonitrile-based HOFs.[44,45] Motivated by these works, we further explored the self-assembly of benzonitrile-based porphyrinic organic linkers in different solvent systems (polar and nonpolar) to gain more insight into the self-assembly mechanism of HOF chemistry. Herein, we report three HOFs, **HOF-26**, **HOF-27**, and **HOF-28**, assembled by a porphyrinic organic linker 4,4′,4″,4‴-(porphyrin-5,10,15,20-tetrayl)tetrabenzonitrile (PTTBN) in ethylbenzene (EB), nitrobenzene (NB), and tetrahydrofuran (THF), respectively, as shown in Scheme 1. We realized fine-tuning the connectivity of PTTBN units and the stacking patterns of H-bonded two-dimensional (2D) layers upon different polarities and molecular structures of guest molecules

Received: February 11, 2022
Revised: April 28, 2022
Published: May 9, 2022

https://doi.org/10.1021/acs.cgd.2c00182
Cryst. Growth Des. 2022, 22, 3808−3814

Scheme 1. Schematic Illustration of Solvent-Dependent Self-Assembly of HOFs

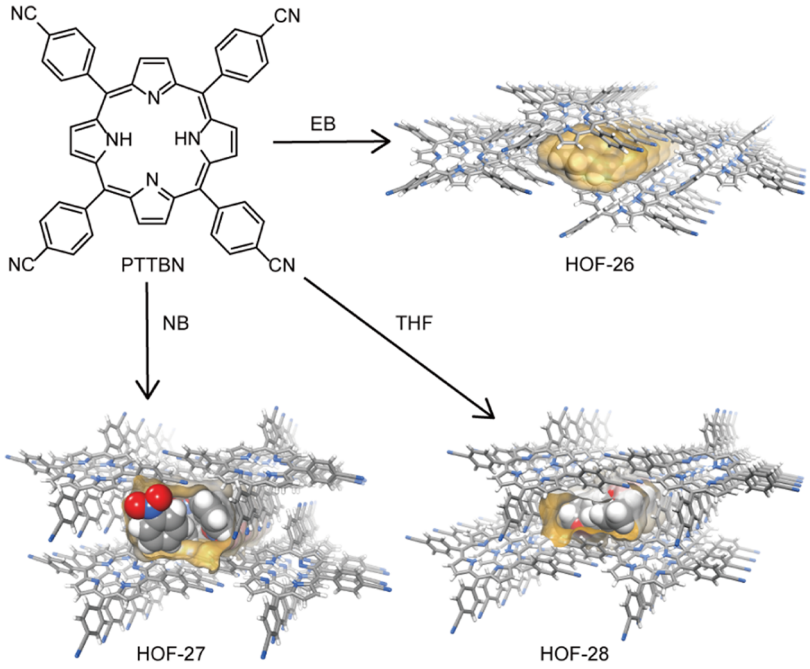

Table 1. Crystallographic Data for HOF-26, HOF-27, and HOF-28

	HOF-26	HOF-27	HOF-28
empirical formula	$C_{48}H_{26}N_8 \cdot C_8H_{10}$	$C_{48}H_{26}N_8 \cdot 2C_6H_5NO_2$	$C_{48}H_{26}N_8 \cdot 2C_4H_8O$
formula weight	820.96	837.90	786.89
crystal system	triclinic	triclinic	triclinic
space group	$P1$	$P\bar{1}$	$P\bar{1}$
a/Å	8.664(10)	11.048(11)	6.605(2)
b/Å	10.835(2)	13.106(15)	10.996(4)
c/Å	12.362(3)	17.261(2)	15.713(6)
α/°	76.20(2)	97.04(10)	100.60(3)
β/°	70.12(2)	102.48(10)	98.97(3)
γ/°	75.14(2)	90.99(9)	90.86(3)
volume (Å^3)	1040.24(4)	2419.59(5)	1107.00(7)
Z	1	2	2
D_{cal} (g/cm^3)	1.310	1.319	1.288
absorption coefficient (mm^{-1})	0.619	0.691	0.637
$F(000)$	428	996	450
goodness-of-fit on F^2	1.053	1.000	1.024
R_1[a], wR_2[b] [$I > 2\sigma(I)$]	$R_1 = 0.0616$, $wR_2 = 0.1329$	$R_1 = 0.0472$, $wR_2 = 0.1157$	$R_1 = 0.0576$, $wR_2 = 0.1189$
R_1[a], wR_2[b] (all data)	$R_1 = 0.0688$, $wR_2 = 0.1382$	$R_1 = 0.0544$, $wR_2 = 0.1208$	$R_1 = 0.0683$, $wR_2 = 0.1244$
largest diff. peak and hole (e/Å^3)	1.530/−0.474	0.586/−0.516	0.334/−0.374

[a] $R_1 = \Sigma(||F_0| - |F_C||)/\Sigma|F_0|$. [b] $wR_2 = [\Sigma w(|F_0|^2 - |F_C|^2)^2/\Sigma w(F_0^2)]^{1/2}$.

employed, which led to distinct pore space and geometries. This work showcases the solvent-dependent self-assembly strategy as a toolkit for pore engineering in HOFs and the development of multifunctional porous materials.

EXPERIMENTAL SECTION

General Remarks. All of the chemicals were purchased commercially (Sigma-Aldrich, Aesar, ACROS) and directly employed as received without further purification unless otherwise mentioned. Reagents were purchased at the highest commercial quality and used without further treatment. ^{1}H NMR spectra were recorded on a Brüker Avance 500 (^{1}H NMR, 500 MHz). TMS was used as an internal standard for ^{1}H NMR (0.00 ppm), and the solvent signal was used as a reference for ^{1}H NMR (dimethyl sulfoxide (DMSO), 2.50 ppm). The powder X-ray diffraction (PXRD) patterns were recorded on a Rigaku SmarLab X-ray powder diffractometer equipped with a Cu sealed tube (λ = 1.54178 Å) at room temperature. Simulation of the PXRD patterns was carried out by the single-crystal data and diffraction-crystal module of the Mercury program at http://www.ccdc.cam.ac.uk/mercury/. The organic linker 4,4′,4″,4‴-(porphyrin-5,10,15,20-tetrayl)tetrabenzonitrile (PTTBN) was synthesized according to our previous work.[44] The gas sorption measurements were carried out on an automatic volumetric adsorption apparatus Micromeritics ASAP 2020 surface area analyzer. Prior to the gas sorption analyses, the samples were activated under a dynamic vacuum at 100 °C for 3 h.

Crystallization of HOFs. 4,4′,4″,4‴-(Porphyrin-5,10,15,20-tetrayl)tetrabenzonitrile (PTTBN) (10 mg) was dissolved in solvents (EB, NB, and THF) (2 mL) after sonication and heating. The resulting supernatant solutions were cooled to room temperature and

https://doi.org/10.1021/acs.cgd.2c00182
Cryst. Growth Des. 2022, 22, 3808−3814

allowed to evaporate at room temperature for 2 weeks. Purple-red rod-shaped crystals were then harvested in the bottom of the vials (yield: 78% for **HOF-26**, 88% for **HOF-27**, 90% for **HOF-28**).

Single-Crystal X-ray Diffraction. The single crystals of **HOF-26**, **HOF-27**, and **HOF-28** suitable for X-ray diffraction were mounted in Paratone oil onto a glass fiber and frozen under a nitrogen cold stream. The data were collected at 100 K using a Rigaku AFC12/Saturn 724 CCD fitted with Cu Kα radiation (λ = 1.54184 Å). Data collection and unit cell refinement were executed using Crystal Clear software. Data processing and absorption correction, giving minimum and maximum transmission factors, were accomplished with CrysAlisPro and SCALE3 ABSPACK, respectively. The structure was solved by direct methods and refined on F^2 using full-matrix least-squares techniques with *SHELXL*. All nonhydrogen atoms were refined with anisotropic displacement parameters. All hydrogen atom positions were determined by geometry and refined by a riding model.

RESULTS AND DISCUSSION

The single crystals of **HOF-26**, **HOF-27**, and **HOF-28** were readily crystallized from the corresponding solvents (EB, NB, and THF, respectively). The phase purities were confirmed by the powder X-ray diffraction patterns, which indicated a good match with the simulated ones (Figure S1). ^{1}H NMR studies of the dissolved HOFs in DMSO-d_6 validated the cocrystallization of EB, NB, and THF molecules with PTTBN in **HOF-26**, **HOF-27**, and **HOF-28**, respectively (Figures S2−S4). The porosity of three HOFs was examined by 77 K nitrogen adsorption analysis. However, the uptake amounts were shown to be lower than those expected from the crystal structures, which is attributed to the collapse of the porous structures (Figure S5).

Crystal Structure of HOF-26/HOF-27/HOF-28. X-ray diffraction studies showed that **HOF-26** crystallizes in the triclinic space group $P\bar{1}$ (Table 1). The asymmetric unit of **HOF-26** is composed of one PTTBN and one doubly disordered EB molecule. Each PTTBN molecule forms four pairs of C−H···N hydrogen bonds (3.325−3.482 Å) to connect with four neighboring linkers, giving a two-dimensional hydrogen-bonded network with **sql** topology (Figure 1a and S6a). Geometrical details about the intermolecular H-bonding interactions within the 2D layers are summarized in Table 2. The adjacent layers are packed in an inclined AB stacking pattern with an interlayer distance of 3.97 Å to encapsulate the intrinsic ellipsoidal cavity embedded in the 2D layers into sandwiched-like pore confinement (12.8 × 8.0 × 4.9 Å^3) (Figures 1b and S8a). The discrete cavity occupied 22.5% of the unit cell volume (1040.24 Å^3). As shown in the simplified topology, the 2D layers are related by displacements along the *a*-axis of 8.66 Å (Figure S7a). The EB molecules are bound tightly within the cavities through weak C−H·· π interactions ($d_{H\cdots C/N}$ = 2.689−2.952 Å) (Figure 1c). Such binding fashion and stacking pattern in **HOF-26** is similar to those observed in our previously published **HOF-29**⊃pX but with a slightly larger cavity size to accommodate the bulkier EB molecule.[44]

HOF-27 crystallizes in the triclinic space group $P\bar{1}$, with one crystallographically unique PTTBN molecule and two different NB molecules in the asymmetric unit. Compared to **HOF-26**, although the sql topology and the number of hydrogen bonding interactions are unaltered, the connectivity of the PTTBN linker observed in **HOF-27** is slightly different: all four pyrrole subunits in the PTTBN are hydrogen-bonded to the neighboring linkers (C−H···N 3.434−3.532 Å), which gives rise to a distorted sql network (interior angle from 62.9°

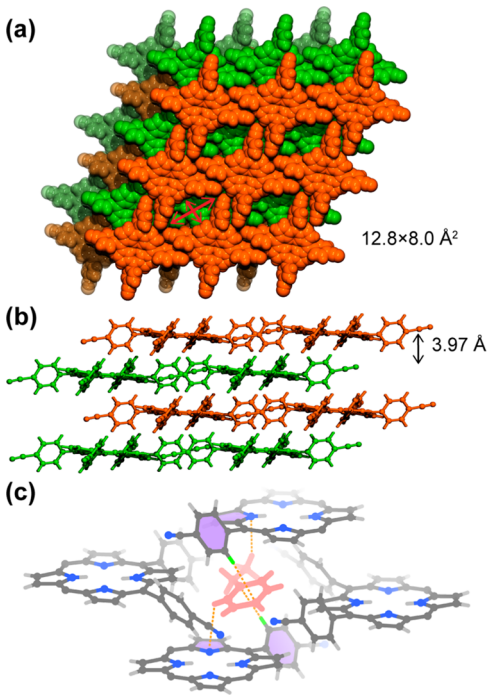

Figure 1. Crystal structure of **HOF-26**. (a) Top view of the packing diagram of the two-dimensional **sql** hydrogen-bonded layers. (b) Side view of the inclined AB stacking patterns with the interlayer distance indicated. The guest EB molecules are omitted for clarity. (c) Perspective view of binding orientation for EB in the pore confinement of **HOF-26**. C−H···π interactions and hydrogen bonding donors from PTTBN are highlighted in orange and light green, respectively.

in **HOF-26** to 87.4° in **HOF-27**) and a round-shaped cavity with a size of 12.2 × 11.0 Å^2 (Figures 2a and S6b). In **HOF-27**, the 2D layers adopt an inclined AA pattern with an elongated interlayer distance of 4.05 Å, allowing the cavities to merge into a one-dimensional channel running along the *b*-axis with a void ratio of 33.5% (unit cell volume of 2419.59 Å^3) (Figures 2b and S8b). The pore size of the channel is 9.8 × 5.6 Å^2. Interestingly, in contrast to the nonpolar ethylbenzene, the high polarity nature of nitrobenzene enables multiple considerably stronger hydrogen bonding interactions to stabilize their orientations: the nitro groups in both NB molecules serve as hydrogen bonding acceptors to interact with multiple phenyl rings and pyrrole units (C−H···N(nitro), $d_{H\cdots N}$ = 2.560−2.713 Å, shorter than 2.75 Å, sum of vdW radii of N and H). In addition, intermolecular C−H···N(nitrile) ($d_{H\cdots N}$ = 2.521−3.083 Å) and C−H··· π interactions ($d_{H\cdots C}$ = 3.115−3.321 Å) are also found between NB molecules and PTTBN linkers. (Figure 2c)

Similarly, **HOF-28** crystallizes in the triclinic space group $P\bar{1}$ with the asymmetric unit consisting of half of one PTTBN and one doubly disordered THF molecule. The connectivity of PTTBN in **HOF-28** is similar to that of **HOF-26**, with half of the pyrrole units extended to other linkers, resulting in an oval-shaped cavity exhibiting a size of 13.3 × 6.5 Å^2 surrounded by two PTTBN molecules (Figure 3a). The hydrogen-bonded layers in **HOF-28** also adopt the inclined AA stacking pattern with a similar interlayer distance (4.02 Å) and interlayer displacement along the *b*-axis of 6.62 Å, as shown in the simplified topology, compared to that of 6.61 Å in **HOF-27** (Figures 3b and S7c). Thereby, the one-dimensional channel

https://doi.org/10.1021/acs.cgd.2c00182
Cryst. Growth Des. 2022, 22, 3808−3814

Table 2. Summary of Hydrogen Bonding Interaction Details and Geometries

HOFs	donor−H···acceptor	H···A (Å)	D−H···A (Å)	angle (deg)
HOF-26	C14−H14A···N7^{i}	2.556	3.341	142
	C38−H38A···N5^{ii}	2.532	3.325	143
	C15−H15A···N8^{iii}	2.595	3.482	160
	C39−H39A···N6	2.599	3.477	157
symmetry codes	(i) 1 + *x*, *y*, 1 + *z*; (ii) 2 + *x*, −1 + *y*, *z*; (iii) 1 + *x*, *y*, 1 + *z*			
HOF-27	C2−H2A···N6^{i}	2.623	3.532	160
	C26−H26A···N8^{ii}	2.470	3.395	164
	C38−H38A···N5^{iii}	2.452	3.376	164
	C14−H14A···N7	2.524	3.434	160
symmetry codes	(i) *x*, *y*, −1 + *z*; (ii) *x*, *y*, *z*; (iii) 1 + *x*, −1 + *y*, *z*			
HOF-28	C3−H3A···N4^{i}	2.546	3.428	158
	C2−H2A···N3^{ii}	2.615	3.523	165
symmetry codes	(i) −*x*, 2 − *y*, −*z*; (ii) 2 − *x*, 2−*y*, 1 − *z*			

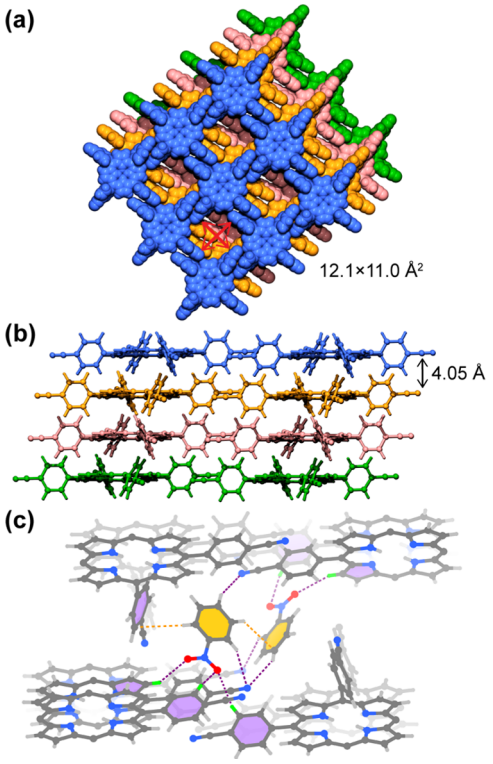

Figure 2. Crystal structure of **HOF-27**. (a) Top view of the packing diagram of the two-dimensional **sql** hydrogen-bonded layers. (b) Side view of the inclined AA stacking patterns with the interlayer distance indicated. The guest NB molecules are omitted for clarity. (c) Perspective view of binding orientation for NB in the pore channel of **HOF-27**. C−H···O/N, C−H···π interactions, and H-bonding donors from PTTBN are highlighted in purple, orange, and light green, respectively.

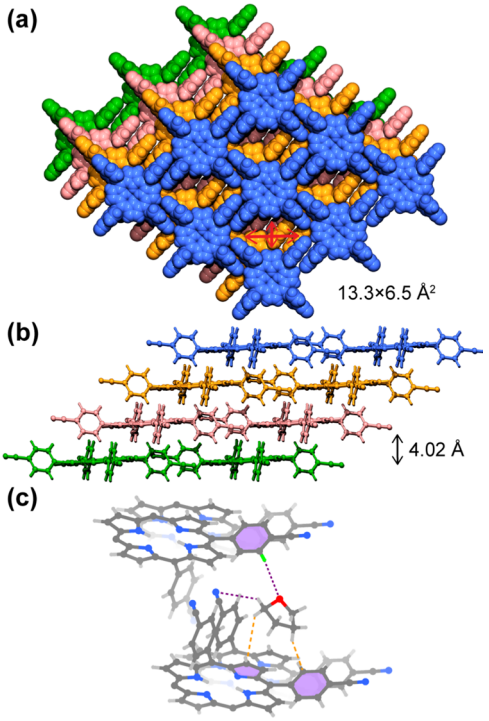

Figure 3. Crystal structure of **HOF-28**. (a) Top view of the packing diagram of the two-dimensional **sql** hydrogen-bonded layers. (b) Side view of the inclined AA stacking patterns with the interlayer distance indicated. The guest THF molecules are omitted for clarity. (c) Perspective view of binding orientation for THF in the pore channel of **HOF-28**. C−H···O/N, C−H···π interactions, and H-bonding donors from PTTBN are highlighted in purple, orange, and light green, respectively.

in **HOF-28** exhibits a pore size of 11.3×5.2 Å^2, which occupies 25.5% of the volume of unit cell (1107.00 Å^3) (Figure S8c). A close inspection on the crystal structure of **HOF-28** reveals that THF molecules reside along the pore channel with the framework through C−H···N(nitrile)/O(THF) and C−H···π interactions ($d_{H\cdots N/O}$ = 3.007, 2.943 and $d_{H\cdots C}$ = 3.156−3.523 Å, respectively) (Figure 3c).

Self-Assembly Mechanism. The slightly different sql hydrogen-bonded layers with distinct local linker distortions (dihedral angles) and stacking patterns shown in three HOFs induced by guest molecules motivated us to investigate the driven forces of the self-assembly of the molecular crystals (Figures S6,S7 and Table S1). As shown in Figure S9, the nitrogen atoms in the porphyrin ring are observed to form weak C−H···N hydrogen bonding interactions in three HOF structures. Besides, $\pi\cdots\pi$ stacking was found in **HOF-27** and **HOF-28** with a distance of 3.71 Å between the porphyrin rings, which led to the formation of the inclined AA stacking patterns accompanied by the interlayer hydrogen bonding. However, there was no $\pi\cdots\pi$ stacking observed in **HOF-26** due to the larger node-to-node distance and the AB stacking pattern. We performed energy decomposition analysis to calculate the interlayer interaction energies using the adjacent PTTBN molecules from two different layers as cluster models

https://doi.org/10.1021/acs.cgd.2c00182
Cryst. Growth Des. 2022, 22, 3808−3814

(Table S2). It can be concluded that the dispersion term is the dominant contributor of the overall interactions between two layers. For **HOF-26**, the overall energy (−89.0 kJ/mol) is significantly lower than those in **HOF-27** (−105.3 kJ/mol) and **HOF-28** (−104.4 kJ/mol) due to the loss of the $\pi\cdots\pi$ stacking, which contributed to the dispersion interaction energy. Such a phenomenon can be rationalized by the fact that the stabilization of nonpolar EB molecules highly relies on the maximum contact with the PTTBN molecules and the AB stacking patterns. On the other hand, the polar guest molecules, NB and THF, are able to form strong guest−guest and/or host−guest interactions to allow the host structure to adopt the more thermodynamically preferred AA stacking patterns. In addition, the intralayer hydrogen bonding interaction energy was also calculated to evaluate its hydrogen bonding nature (Figure S10). In this case, a total energy of −56.3 kJ/mol was obtained for two pairs of C−H···NC hydrogen bonds with higher electrostatic component than the dispersion term, which contrasts with the interlayer interactions and verified its moderate bonding energy according to the classification of Jeffrey and Steiner.[46]

CONCLUSIONS

In summary, we have successfully realized solvent-dependent self-assembly of a series of microporous hydrogen-bonded organic frameworks (HOFs), **HOF-26**, **HOF-27**, and **HOF-28**, from a porphyrinic organic linker PTTBN in different solvents, ethylbenzene, nitrobenzene, and THF, respectively. Single-crystal X-ray diffraction studies reveal that the PTTBN linkers are held together by the intermolecular hydrogen bonding interactions from nitrile groups into two-dimensional extended networks. The 2D layers are further stacked compactly in an AB pattern to encapsulate nonpolar EB molecules and in an AA pattern to accommodate polar NB and THF molecules with different pore geometries. The flexible nature of the linker and its solvent-dependent self-assembly offers the platform to engineer the overall HOF structure and pore environment. This work will facilitate the future exploration of nitrile-based HOFs and show the promise to develop tailor-made HOFs with a well-defined pore structure for more specific applications.

ASSOCIATED CONTENT

Supporting Information

The Supporting Information is available free of charge at https://pubs.acs.org/doi/10.1021/acs.cgd.2c00182.

X-ray crystallographic files (CIF), powder X-ray diffraction analysis (PXRD), and NMR spectra of **HOF-26**, **HOF-27**, and **HOF-28** (PDF)

Accession Codes

CCDC 2151428−2151430 contain the supplementary crystallographic data for this paper. These data can be obtained free of charge via www.ccdc.cam.ac.uk/data_request/cif, or by emailing data_request@ccdc.cam.ac.uk, or by contacting The Cambridge Crystallographic Data Centre, 12 Union Road, Cambridge CB2 1EZ, UK; fax: +44 1223 336033.

AUTHOR INFORMATION

Corresponding Authors

Yi Xie − *Department of Chemistry, University of Texas at San Antonio, San Antonio, Texas 78249-0698, United States*; Email: yi.xie@utsa.edu

Banglin Chen − *Department of Chemistry, University of Texas at San Antonio, San Antonio, Texas 78249-0698, United States*; orcid.org/0000-0001-8707-8115; Email: banglin.chen@utsa.edu

Authors

Li Ma − *Department of Chemistry, University of Texas at San Antonio, San Antonio, Texas 78249-0698, United States*

Hadi Arman − *Department of Chemistry, University of Texas at San Antonio, San Antonio, Texas 78249-0698, United States*

Wei Zhou − *Center for Neutron Research, National Institute of Standards and Technology, Gaithersburg, Maryland 20899-6102, United States*; orcid.org/0000-0002-5461-3617

Complete contact information is available at: https://pubs.acs.org/10.1021/acs.cgd.2c00182

Notes

The authors declare no competing financial interest.

ACKNOWLEDGMENTS

The authors are grateful for financial support from the Welch Foundation (AX-1730). L.M. thanks the generous support from the Presidential Distinguished Research Fellowship (PDRF) of the University of Texas at San Antonio (UTSA). The single-crystal X-ray diffraction experiments conducted at UTSA were supported by the U.S. National Science Foundation (MRI 1920057).

REFERENCES

(1) Alberts, B.; Johnson, A.; Lewis, J.; Raff, M.; Roberts, K.; Walter, P. *Mol. Biol. Cell*, 4th ed.; Taylor and Francis, 2002.

(2) Lin, R.-B.; He, Y.; Li, P.; Wang, H.; Zhou, W.; Chen, B. Multifunctional porous hydrogen-bonded organic framework materials. *Chem. Soc. Rev.* **2019**, *48*, 1362−1389.

(3) Li, P.; Ryder, M. R.; Stoddart, J. F. Hydrogen-Bonded Organic Frameworks: A Rising Class of Porous Molecular Materials. *Acc. Mater. Res.* **2020**, *1*, 77−87.

(4) Hisaki, I.; Xin, C.; Takahashi, K.; Nakamura, T. Designing Hydrogen-Bonded Organic Frameworks (HOFs) with Permanent Porosity. *Angew. Chem., Int. Ed.* **2019**, *58*, 11160−11170.

(5) Luo, J.; Wang, J.-W.; Zhang, J.-H.; Lai, S.; Zhong, D.-C. Hydrogen-bonded organic frameworks: design, structures and potential applications. *CrystEngComm* **2018**, *20*, 5884−5898.

(6) Diercks, C. S.; Yaghi, O. M. The atom, the molecule, and the covalent organic framework. *Science* **2017**, *355*, No. eaal1585.

(7) Furukawa, H.; Cordova, K. E.; O'Keeffe, M.; Yaghi, O. M. The chemistry and applications of metal-organic frameworks. *Science* **2013**, *341*, No. 1230444.

(8) Lin, R.-B.; Zhang, Z.; Chen, B. Achieving High Performance Metal−Organic Framework Materials through Pore Engineering. *Acc. Chem. Res.* **2021**, *54*, 3362−3376.

(9) Luo, X.-Z.; Jia, X.-J.; Deng, J.-H.; Zhong, J.-L.; Liu, H.-J.; Wang, K.-J.; Zhong, D.-C. A Microporous Hydrogen-Bonded Organic Framework: Exceptional Stability and Highly Selective Adsorption of Gas and Liquid. *J. Am. Chem. Soc.* **2013**, *135*, 11684−11687.

(10) Zhang, X.; Li, L.; Wang, J.-X.; Wen, H.-M.; Krishna, R.; Wu, H.; Zhou, W.; Chen, Z.-N.; Li, B.; Qian, G.; Chen, B. Selective Ethane/Ethylene Separation in a Robust Microporous Hydrogen-Bonded Organic Framework. *J. Am. Chem. Soc.* **2020**, *142*, 633−640.

(11) Ye, Z.-M.; Zhang, X.-W.; Liao, P.-Q.; Xie, Y.; Xu, Y.-T.; Zhang, X.-F.; Wang, C.; Liu, D.-X.; Huang, N.-Y.; Qiu, Z.-H.; Zhou, D.-D.; He, C.-T.; Zhang, J.-P. A Hydrogen-Bonded yet Hydrophobic Porous Molecular Crystal for Molecular-Sieving-like Separation of Butane and Isobutane. *Angew. Chem., Int. Ed.* **2020**, *59*, 23322−23328.

(12) Bao, Z.; Xie, D.; Chang, G.; Wu, H.; Li, L.; Zhou, W.; Wang, H.; Zhang, Z.; Xing, H.; Yang, Q.; Zaworotko, M. J.; Ren, Q.; Chen, B. Fine Tuning and Specific Binding Sites with a Porous Hydrogen-Bonded Metal-Complex Framework for Gas Selective Separations. *J. Am. Chem. Soc.* **2018**, *140*, 4596−4603.
(13) Gao, J.; Cai, Y.; Qian, X.; Liu, P.; Wu, H.; Zhou, W.; Liu, D.-X.; Li, L.; Lin, R.-B.; Chen, B. A Microporous Hydrogen-Bonded Organic Framework for the Efficient Capture and Purification of Propylene. *Angew. Chem., Int. Ed.* **2021**, *60*, 20400−20406.
(14) Kang, D. W.; Kang, M.; Kim, H.; Choe, J. H.; Kim, D. W.; Park, J. R.; Lee, W. R.; Moon, D.; Hong, C. S. A Hydrogen-Bonded Organic Framework (HOF) with Type IV NH_3 Adsorption Behavior. *Angew. Chem., Int. Ed.* **2019**, *58*, 16152−16155.
(15) Li, P.; He, Y.; Guang, J.; Weng, L.; Zhao, J. C.-G.; Xiang, S.; Chen, B. A Homochiral Microporous Hydrogen-Bonded Organic Framework for Highly Enantioselective Separation of Secondary Alcohols. *J. Am. Chem. Soc.* **2014**, *136*, 547−549.
(16) Gong, W.; Chu, D.; Jiang, H.; Chen, X.; Cui, Y.; Liu, Y. Permanent porous hydrogen-bonded frameworks with two types of Brønsted acid sites for heterogeneous asymmetric catalysis. *Nat. Commun.* **2019**, *10*, No. 600.
(17) Han, B.; Wang, H.; Wang, C.; Wu, H.; Zhou, W.; Chen, B.; Jiang, J. Postsynthetic Metalation of a Robust Hydrogen-Bonded Organic Framework for Heterogeneous Catalysis. *J. Am. Chem. Soc.* **2019**, *141*, 8737−8740.
(18) Yu, B.; Li, L.; Liu, S.; Wang, H.; Liu, H.; Lin, C.; Liu, C.; Wu, H.; Zhou, W.; Li, X.; Wang, T.; Chen, B.; Jiang, J. Robust Biological Hydrogen-Bonded Organic Framework with Post-Functionalized Rhenium(I) Sites for Efficient Heterogeneous Visible-Light-Driven CO2 Reduction. *Angew. Chem., Int. Ed.* **2021**, *60*, 8983−8989.
(19) Wang, B.; He, R.; Xie, L.-H.; Lin, Z.-J.; Zhang, X.; Wang, J.; Huang, H.; Zhang, Z.; Schanze, K. S.; Zhang, J.; Xiang, S.; Chen, B. Microporous Hydrogen-Bonded Organic Framework for Highly Efficient Turn-Up Fluorescent Sensing of Aniline. *J. Am. Chem. Soc.* **2020**, *142*, 12478−12485.
(20) Hisaki, I.; Suzuki, Y.; Gomez, E.; Ji, Q.; Tohnai, N.; Nakamura, T.; Douhal, A. Acid Responsive Hydrogen-Bonded Organic Frameworks. *J. Am. Chem. Soc.* **2019**, *141*, 2111−2121.
(21) Liang, W.; Carraro, F.; Solomon, M. B.; Bell, S. G.; Amenitsch, H.; Sumby, C. J.; White, N. G.; Falcaro, P.; Doonan, C. J. Enzyme Encapsulation in a Porous Hydrogen-Bonded Organic Framework. *J. Am. Chem. Soc.* **2019**, *141*, 14298−14305.
(22) Feng, S.; Shang, Y.; Wang, Z.; Kang, Z.; Wang, R.; Jiang, J.; Fan, L.; Fan, W.; Liu, Z.; Kong, G.; Feng, Y.; Hu, S.; Guo, H.; Sun, D. Fabrication of a Hydrogen-Bonded Organic Framework Membrane through Solution Processing for Pressure-Regulated Gas Separation. *Angew. Chem., Int. Ed.* **2020**, *59*, 3840−3845.
(23) Hu, F.; Liu, C.; Wu, M.; Pang, J.; Jiang, F.; Yuan, D.; Hong, M. An Ultrastable and Easily Regenerated Hydrogen-Bonded Organic Molecular Framework with Permanent Porosity. *Angew. Chem., Int. Ed.* **2017**, *56*, 2101−2104.
(24) Mastalerz, M.; Oppel, I. M. Rational Construction of an Extrinsic Porous Molecular Crystal with an Extraordinary High Specific Surface Area. *Angew. Chem., Int. Ed.* **2012**, *51*, 5252−5255.
(25) Wang, B.; Lin, R.-B.; Zhang, Z.; Xiang, S.; Chen, B. Hydrogen-Bonded Organic Frameworks as a Tunable Platform for Functional Materials. *J. Am. Chem. Soc.* **2020**, *142*, 14399−14416.
(26) Pulido, A.; Chen, L.; Kaczorowski, T.; Holden, D.; Little, M. A.; Chong, S. Y.; Slater, B. J.; McMahon, D. P.; Bonillo, B.; Stackhouse, C. J.; Stephenson, A.; Kane, C. M.; Clowes, R.; Hasell, T.; Cooper, A. I.; Day, G. M. Functional materials discovery using energy−structure−function maps. *Nature* **2017**, *543*, 657−664.
(27) Brunet, P.; Simard, M.; Wuest, J. D. Molecular Tectonics. Porous Hydrogen-Bonded Networks with Unprecedented Structural Integrity. *J. Am. Chem. Soc.* **1997**, *119*, 2737−2738.
(28) He, Y.; Xiang, S.; Chen, B. A Microporous Hydrogen-Bonded Organic Framework for Highly Selective C_2H_2/C_2H_4 Separation at Ambient Temperature. *J. Am. Chem. Soc.* **2011**, *133*, 14570−14573.
(29) Li, P.; He, Y.; Zhao, Y.; Weng, L.; Wang, H.; Krishna, R.; Wu, H.; Zhou, W.; O'Keeffe, M.; Han, Y.; Chen, B. A Rod-Packing Microporous Hydrogen-Bonded Organic Framework for Highly Selective Separation of C_2H_2/CO_2 at Room Temperature. *Angew. Chem., Int. Ed.* **2015**, *54*, 574−577.
(30) Wang, H.; Li, B.; Wu, H.; Hu, T.-L.; Yao, Z.; Zhou, W.; Xiang, S.; Chen, B. A Flexible Microporous Hydrogen-Bonded Organic Framework for Gas Sorption and Separation. *J. Am. Chem. Soc.* **2015**, *137*, 9963−9970.
(31) Yu, B.; Geng, S.; Wang, H.; Zhou, W.; Zhang, Z.; Chen, B.; Jiang, J. A Solid Transformation into Carboxyl Dimers Based on a Robust Hydrogen-Bonded Organic Framework for Propyne/Propylene Separation. *Angew. Chem., Int. Ed.* **2021**, *60*, 25942−25948.
(32) Wang, B.; Lv, X.-L.; Lv, J.; Ma, L.; Lin, R.-B.; Cui, H.; Zhang, J.; Zhang, Z.; Xiang, S.; Chen, B. A novel mesoporous hydrogen-bonded organic framework with high porosity and stability. *Chem. Commun.* **2020**, *56*, 66−69.
(33) Li, Y.-L.; Alexandrov, E. V.; Yin, Q.; Li, L.; Fang, Z.-B.; Yuan, W.; Proserpio, D. M.; Liu, T.-F. Record Complexity in the Polycatenation of Three Porous Hydrogen-Bonded Organic Frameworks with Stepwise Adsorption Behaviors. *J. Am. Chem. Soc.* **2020**, *142*, 7218−7224.
(34) Hisaki, I.; Nakagawa, S.; Tohnai, N.; Miyata, M. A C3-Symmetric Macrocycle-Based, Hydrogen-Bonded, Multiporous Hexagonal Network as a Motif of Porous Molecular Crystals. *Angew. Chem., Int. Ed.* **2015**, *54*, 3008−3012.
(35) Hashim, M. I.; Le, H. T. M.; Chen, T.-H.; Chen, Y.-S.; Daugulis, O.; Hsu, C.-W.; Jacobson, A. J.; Kaveevivitchai, W.; Liang, X.; Makarenko, T.; Miljanić, O. Š.; Popovs, I.; Tran, H. V.; Wang, X.; Wu, C.-H.; Wu, J. I. Dissecting Porosity in Molecular Crystals: Influence of Geometry, Hydrogen Bonding, and $[\pi\cdots\pi]$ Stacking on the Solid-State Packing of Fluorinated Aromatics. *J. Am. Chem. Soc.* **2018**, *140*, 6014−6026.
(36) Chen, T.-H.; Popov, I.; Kaveevivitchai, W.; Chuang, Y.-C.; Chen, Y.-S.; Daugulis, O.; Jacobson, A. J.; Miljanić, O. Š. Thermally robust and porous noncovalent organic framework with high affinity for fluorocarbons and CFCs. *Nat. Commun.* **2014**, *5*, No. 5131.
(37) Zhou, D.-D.; Xu, Y.-T.; Lin, R.-B.; Mo, Z.-W.; Zhang, W.-X.; Zhang, J.-P. High-symmetry hydrogen-bonded organic frameworks: air separation and crystal-to-crystal structural transformation. *Chem. Commun.* **2016**, *52*, 4991−4994.
(38) Adachi, T.; Ward, M. D. Versatile and Resilient Hydrogen-Bonded Host Frameworks. *Acc. Chem. Res.* **2016**, *49*, 2669−2679.
(39) Lü, J.; Perez-Krap, C.; Suyetin, M.; Alsmail, N. H.; Yan, Y.; Yang, S.; Lewis, W.; Bichoutskaia, E.; Tang, C. C.; Blake, A. J.; Cao, R.; Schröder, M. A Robust Binary Supramolecular Organic Framework (SOF) with High CO_2 Adsorption and Selectivity. *J. Am. Chem. Soc.* **2014**, *136*, 12828−12831.
(40) Huang, Q.; Li, W.; Mao, Z.; Qu, L.; Li, Y.; Zhang, H.; Yu, T.; Yang, Z.; Zhao, J.; Zhang, Y.; Aldred, M. P.; Chi, Z. An exceptionally flexible hydrogen-bonded organic framework with large-scale void regulation and adaptive guest accommodation abilities. *Nat. Commun.* **2019**, *10*, No. 3074.
(41) Hou, L.; Shan, C.; Song, Y.; Chen, S.; Wojtas, L.; Ma, S.; Sun, Q.; Zhang, L. Highly Stable Single Crystals of Three-Dimensional Porous Oligomer Frameworks Synthesized under Kinetic Conditions. *Angew. Chem. Int. Ed.* **2021**, *60*, 14664−14670.
(42) Li, P.; Li, P.; Ryder, M. R.; Liu, Z.; Stern, C. L.; Farha, O. K.; Stoddart, J. F. Interpenetration Isomerism in Triptycene-Based Hydrogen-Bonded Organic Frameworks. *Angew. Chem., Int. Ed.* **2019**, *58*, 1664−1669.
(43) Wang, H.; Bao, Z.; Wu, H.; Lin, R.-B.; Zhou, W.; Hu, T.-L.; Li, B.; Zhao, J. C.-G.; Chen, B. Two solvent-induced porous hydrogen-bonded organic frameworks: solvent effects on structures and functionalities. *Chem. Commun.* **2017**, *53*, 11150−11153.
(44) Ma, L.; Xie, Y.; Khoo, R. S. H.; Arman, H.; Wang, B.; Zhou, W.; Zhang, J.; Lin, R.-B.; Chen, B. An Adaptive Hydrogen-Bonded Organic Framework for the Exclusive Recognition of p-Xylene. *Chem. − Eur. J.* **2022**, *28*, No. e202104269.

https://doi.org/10.1021/acs.cgd.2c00182
Cryst. Growth Des. 2022, 22, 3808−3814

(45) Yang, Y.; Li, L.; Lin, R.-B.; Ye, Y.; Yao, Z.; Yang, L.; Xiang, F.; Chen, S.; Zhang, Z.; Xiang, S.; Chen, B. Ethylene/ethane separation in a stable hydrogen-bonded organic framework through a gating mechanism. *Nat. Chem.* **2021**, *13*, 933−939.
(46) Steiner, T. The Hydrogen Bond in the Solid State. *Angew. Chem., Int. Ed.* **2002**, *41*, 48−76.

https://doi.org/10.1021/acs.cgd.2c00182
Cryst. Growth Des. 2022, 22, 3808−3814